Electronic Supplementary Material (ESI) for Physical Chemistry Chemical Physics.

Electronic Supplementary Information

Two-dimensional $ErCu_2$ intermetallic compound on Cu(111) with moiré-pattern-modulated electronic structures

Chaoqiang Xu,[a] Kejie Bao,[a] Yande Que,[a] Yuan Zhuang,[a] Xiji Shao,[b] Kedong Wang,[b,c]

Junyi Zhu*[a] and Xudong Xiao*[a]

[a] *Department of Physics, the Chinese University of Hong Kong, Shatin, Hong Kong, China*

[b] *Department of Physics, Southern University of Science and Technology, Shenzhen, Guangdong 518055, P. R. China*

[c] *Shenzhen Key Laboratory of Quantum Science and Engineering, SUSTech, Shenzhen 518055, China*

* Corresponding author.

Email: jyzhu@phy.cuhk.edu.hk, xdxiao@phy.cuhk.edu.hk

1. Sample Preparation

Our experiment was carried out in an ultrahigh vacuum (UHV) chamber (base pressure of 5×10^{-11} mbar) equipped with an Omicron low-temperature scanning tunneling microscope (LT-STM), an argon ion sputtering source, a sample stage with electron beam heating, and an evaporator of Er source. Atomically flat Cu(111) clean surface with large terraces (about 150 nm) was prepared by repeated cycles of Ar^+ sputtering and annealing at 700 K. Er atoms were evaporated, from an erbium rod (Goodfellow, 99%) heated by electron bombardment, to the Cu(111) surface at room temperature at a deposition rate of about 0.05 monolayers per minute (ML/min). Prior to evaporation, the rod was thoroughly degassed for about 100 hours to obtain a chamber pressure below 1×10^{-10} mbar during deposition. After deposition, the sample was annealed at 473 K for 30 min followed by slow cooling back to room temperature (4 K/min). Then, the sample was transferred to the analysis chamber and further cooled down to liquid nitrogen temperature (~ 77 K) for STM imaging.

2. STM/STS measurement methods

The STM tip was an electrochemically etched tungsten tip, which was further modified by gently touching the tip on the clean metal surface, presumably removing the oxides of the tip surface. The density of state (DOS) of the tip was ensured flat within reasonable energy range by checking the tunneling spectra of Cu(111) to reliably and accurately reproduce the well-known characteristic conductance signature of the Cu(111) surface state.[1] The spectroscopic dI/dV data

were obtained by a lock-in technique with a small peak-to-peak modulation of 2 mV. The STM images were processed and analyzed using WSxM software.[2] Image scales were calibrated on a well-defined $Si(111)-(7\times7)$ surface. The set point bias voltages here referred to the sample bias.

3. DFT Calculations

The calculations on the structure and electronic states of $ErCu_2$/Cu(111) were based on density functional theory (DFT). We calculated the electronic structure using Vienna Ab-initio Simulation Package (VASP),[3,4] within the Perdew-Burke-Ernzerhopf (PBE) generalized-gradient approximation (GGA).[5] Projector-augmented-wave (PAW) [6,7] pseudopotentials of Cu_pv and Er_3 were used. In rare earth metal calculation, we followed the standard treatment in previous literatures [8,9] that uses $4f^{N-1}5d$ configuration because of the extending property of 5d orbital. Since the Er_3 pseudopotential treats the erbium f states $4f^{11}$) as core states, the deep 4f electrons of Er atom are ignored in such a treatment. Plane waves with a kinetic energy cutoff of 400 eV were used as basis sets and Gamma point sampling in the supercell structure of the moiré pattern was tested. Different Hubbard U values (0 eV or 4 eV) acting on the Cu 3d orbitals were tested to match the experimental data. Spin orbital coupling (SOC) was included in the calculations of electronic structures because of the heavy mass of Er atom.

A tri-layer model was constructed to simulate the moiré pattern, corresponding to a (9×9) unit cell of $ErCu_2$ that was rotated by $30°$ from a Cu(111) surface of the underlying (10×10) Cu bilayer. Among the 81 atoms of the top layer, 27 atoms

are Er, and 54 atoms are Cu. The Cu atoms form a honeycomb lattice, with the Er atoms occupying the centers of the honeycomb. We tested various stacking configurations and found out that the HCP stacking of the top layer is the most energetically favorable one. In the optimization, the top two layers were relaxed, but the third Cu layer was fixed. A minimum of 15 Å of vacuum was used to separate the slabs, in order to reduce the interaction between periodic images. The in-plane lattice constant was fixed at 25.6 Å (10× bulk DFT value 2.56 Å for Cu). Convergence tests based on k-points sampling and vacuum were also performed. For the empty- and filled-state STM image simulations, to better reproduce the experimental STM images, we sampled the electronic configurations 10 meV above and 100 meV below the Fermi level, respectively, with the tip positioned at 1.5 Å above the surface. More calculated STM images at different energies are also presented in Fig. S1. STM simulation in DFT calculation actually is the certain band projection in real space. For empty states, according to our calculation, there are only two degenerate bands in the energy window from 1 to 800 meV, which means STM simulation at any energy level in this window will yield the same results, as shown in Figs. S1a and S1b. However, for STM simulation at filled states, some noticeable changes in the calculated STM images when energy levels drop to below -30 meV, as shown in Figs. S1c-i. The discrepancies between the experimental and calculated results are explainable when considering the approximations used in our calculations. First, limited by the general computing power of DFT, our model can only include 1 layer of $ErCu_2$ and 2 layers of Cu atoms because spin-orbital

coupling (SOC) calculation is too challenging for further increasing the number of atoms involved. Second, we used 4f10 5d model to deal with rare earth metal Er atoms rather than consider all f electrons, which is standard treatment because the inclusion of f electrons often leads to divergence. Finally, a slight deviation from the exact moiré pattern may also lead to some finite differences. Nevertheless, our conclusion is qualitatively solid and reveals the physical essence of STM images.

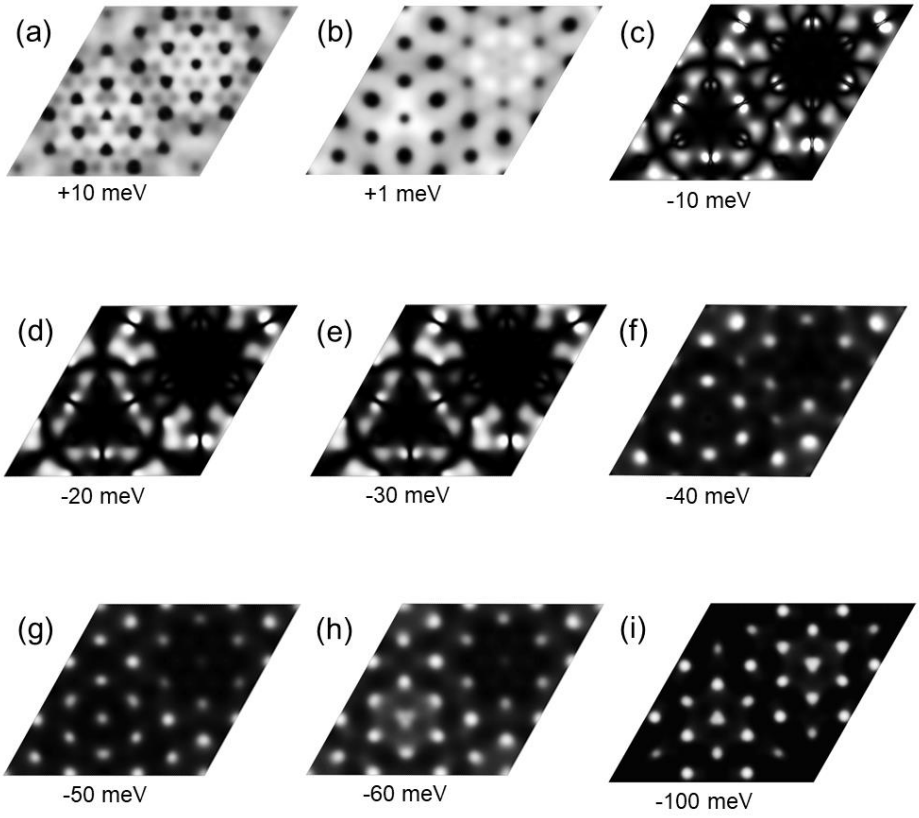

Fig. S1 Calculated STM images at different energy levels

4. Suggested mechanism for surface Er-Cu alloy/compound formation

As shown in Fig. S2a, Er atoms form flat branched islands during deposition on Cu(111) surface at room temperature, implying a much higher energy barrier for exchange of a Er adatom with a Cu surface atom as compared to that for Er diffusion.

Raising the substrate temperature makes it possible for atom exchange between Er islands and Cu(111) surface, leading to the formation of corrugated surface alloy islands having similar shapes but rounded corners [Fig. S2b]. During the second-round deposition, the growth behaviors of Er atoms are governed by the modified edge structures of the existing Er islands as the post-deposition effects take place, resulting in the island growth along the out-of-plane direction and in the perpendicular direction of the previous island edges within-the-plane. Figure S2c presents the consequent formation of multilayer fractal-like Er island. Upon annealing treatment, semi-free Er atoms atop the island move across the boundary and diffuse on Cu(111) surface where they meet the diffusing Cu adatoms, forming a stoichiometric nucleation center, namely, $ErCu_2$. Further attachment of dissociated Er atoms from island edges and Cu adatoms from underlying substrate to the nucleation center leads to the in-plane growth of an extended well-ordered surface structure [Fig. S2d].

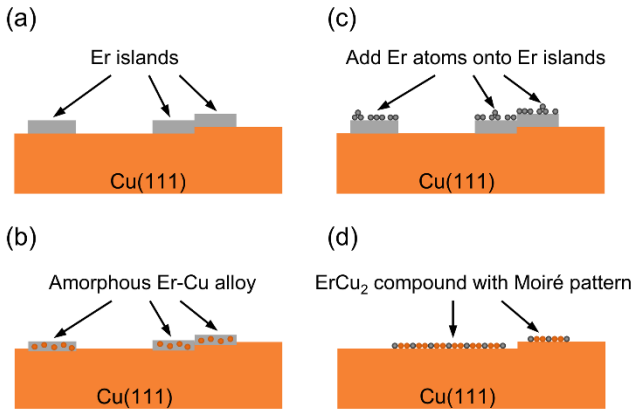

Fig. S2 Schematic models of (a) as-deposited Er islands on Cu(111); (b) amorphous Er-Cu surface alloy formed upon annealing of Er islands in (a); (c) multilayer Er islands resulting from the interrupted deposition of Er on Cu(111); and (d) well-ordered $ErCu_2$ compound exhibiting a hexagonal moiré pattern formed upon annealing of Er islands in (c).

References

1. M. F. Crommie, C. P. Lutz and D. M. Eigler, *Nature*, 1993, **363**, 524-527.
2. I. Horcas, R. Fernández, J. Gomez-Rodriguez, J. Colchero, J. Gómez-Herrero and A. Baro, *Rev. Sci. Instrum.*, 2007, **78**, 013705.
3. G. Kresse and J. Hafner, *Phys. Rev. B*, 1994, **49**, 14251.
4. G. Kresse and J. Furthmüller, *Comput. Mater. Sci.*, 1996, **6**, 15-50.
5. J. P. Perdew, K. Burke and M. Ernzerhof, *Phys. Rev. Lett.*, 1996, **77**, 3865.
6. P. E. Blöchl, *Phys. Rev. B*, 1994, **50**, 17953.
7. G. Kresse and D. Joubert, *Phys. Rev. B*, 1999, **59**, 1758.
8. G. Allan, I. Lefebvre and N. Christensen, *Phys. Rev. B*, 1993, **48**, 8572.
9. C. Thiel, Y. Sun and R. Cone, *Journal of Modern Optics*, 2002, **49**, 2399-2412.